Applied Catalysis B: Environmental 142–143 (2013) 149–160

Contents lists available at SciVerse ScienceDirect

Applied Catalysis B: Environmental

journal homepage: www.elsevier.com/locate/apcatb

Influence of hierarchically porous niobium doped TiO_2 supports in the total catalytic oxidation of model VOCs over noble metal nanoparticles

J.C. Rooke[a,*,1], T. Barakat[b,1], M. Franco Finol[c,1], P. Billemont[d], G. De Weireld[d,2], Y. Li[e], R. Cousin[b], J.-M. Giraudon[c], S. Siffert[b,3], J.-F. Lamonier[c,4], B.L. Su[a,e,**]

[a] Laboratory of Inorganic Materials Chemistry (CMI), University of Namur, 61 rue de Bruxelles, B-5000 Namur, Belgium
[b] Unité de Chimie Environnementale et Interactions sur le Vivant (UCEIV), EA 4492, Université du Littoral-Côte d'Opale, 145 Avenue Maurice Schumann, 59140 Dunkerque, France
[c] Unité de Catalyse et Chimie du Solide, UMR CNRS 8181, Université des Sciences et Technologies, 59655 Villeneuve d'Ascq, France
[d] Faculté Polytechnique de Mons, Université de Mons (UMons), 20 Place du Parc, B-7000 Mons, Belgium
[e] State Key Laboratory of Advanced Technology for Materials Synthesis and Processing, Wuhan University of Technology, 122 Luoshi Road, 430070 Wuhan, China

ARTICLE INFO

Article history:
Received 6 February 2013
Received in revised form 1 May 2013
Accepted 8 May 2013
Available online 15 May 2013

Keywords:
Hierarchical porous supports
VOCs
Niobium doped titania
Noble metal catalysts

ABSTRACT

An Nb doped, hierarchically micro(meso)macroporous TiO_2 (anatase phase) was synthesised via a facile self-formation procedure and employed as a catalytic support, combining the advantages of a promoter with improved diffusion through the intrinsic macroporous network. The efficiency of the catalytic systems in the total oxidation of butan-1-ol and toluene was determined. Niobium was found to promote catalytic activity, with minimal secondary products. Indications suggest that reduction of the catalyst occurs at lower temperatures with an Nb dopant owing to stronger support–metal interactions, which boosts efficiency. This study found that noble metals, Pd and Pt, behave differently when deposited on Nb–TiO_2 with Pt benefiting most from Nb doping, with a marked increase in activity and CO_2 selectivity whereas Pd catalysts have improved low temperature activities. This work highlights the feasibility of economic and energetic reductions by minimising catalyst loading in favour of cheaper catalytic promoters and a reduction in operational temperature during VOC remediation.

1. Introduction

The removal of volatile organic compounds (VOCs), major contributors to atmospheric pollution, at source is ideal. Catalytically aided oxidation is a preferred method over thermal combustion owing to lower processing temperatures and also a higher selectivity [1]. Lowering the temperature at which these processes occur with greatest efficiency can reduce energy costs. Boosting the catalyst loading can decrease reaction temperature; however the noble metals used are costly and scarce. Therefore, it is common to look at the chemical and structural compositions of the catalyst support to increase performance.

Hubbard et al. [2], on investigating the activities of Pt impregnated non-porous supports (ZrO_2 and γAl_2O_3) in propane oxidation, noted that oxidation was twice as fast over Pt/ZrO_2 than $Pt/\gamma Al_2O_3$ owing to different interactions between the support and the catalyst as at higher Pt loadings the effect of the support vanishes. Okumura et al. [3] studied a range of Pd impregnated supports (Al_2O_3, Nb_2O_5, SiO_2, SnO_2, WO_3 and ZrO_2) in toluene combustion and found that the acid–base properties of the support influenced the interaction between catalyst and support, which in turn controlled the activity of Pd. Pd/Al_2O_3 was found to have a greater conversion rate at lower temperatures in the total oxidation of test chlorinated VOCs compared to Pt/Al_2O_3 and even the alumina support alone showed some catalytic activity, owing to the role its surface acidity plays in adsorption of the chlorocarbon via H-bonding. However, although Pd was more active, Pt had a greater selectivity towards CO_2 with more CO produced on using Pd [4]. This highlights that when designing a catalytic system, attention must be paid to the off stream products after destruction of the VOC. Other diverse supports have also been trialled such as the perovskite $LaMO_3$ (M = Mn, Fe, Co), where all three analogues were

* Corresponding author. Tel.: +32 81 724531; fax: +32 81 725414.
** Corresponding author at: Laboratory of Inorganic Materials Chemistry (CMI), University of Namur, 61 rue de Bruxelles, B-5000 Namur, Belgium. Tel.: +32 81 724531; fax: +32 81 725414.
E-mail addresses: joanna.rooke@fundp.ac.be (J.C. Rooke), jean-francois.lamonier@univ-lille1.fr (M.F. Finol), guy.deweireld@umons.ac.be (G. De Weireld), siffert@univ-littoral.fr (S. Siffert), bao-lian.su@fundp.ac.be (B.L. Su).
[1] These authors contributed equally to this work.
[2] Tel.: +32 65 374203.
[3] Tel.: +33 3 20434950.
[4] Tel.: +33 3 28658256.

0926-3373/$ – see front matter © 2013 Elsevier B.V. All rights reserved.
http://dx.doi.org/10.1016/j.apcatb.2013.05.009

found to be better at activating the C—H bond cleavage of hexane than 3% PdO/Al_2O_3 in the total oxidation of hexane [5]. The authors attribute this to a low energy mechanism involving mobile surface oxygen. Activated carbon has been used as a Pt support and tested in the total oxidation of BTX (benzene, toluene and xylene) [6]. It is thought that activated carbon can concentrate VOCs owing, perhaps, to their adsorption capabilities. In this study the light-off temperatures, the initiation temperature of a catalytic reaction, were well below those of a comparison catalyst Pt/Al_2O_3 at 130–150 °C.

A series of oxidised and reduced Pd/TiO_2 catalysts were tested in room temperature formaldehyde oxidation with nearly a 100% conversion attained for the reduced catalyst, which was attributed to a strong metal-support interaction, a good dispersion of Pd nanoparticles and zones rich in chemisorbed oxygen [7]. Various noble metal catalysts (Au, Ir, Pd, Pt and Ru) with TiO_2 as a support have been studied in the oxidation of CO, ethanol and toluene [8]. Firstly catalyst preparation was investigated and it was found that catalyst deposition is strongly influenced by the elaboration method which in turn affects catalyst performance, with liquid phase reduction deposition yielding a more active metallic phase than incipient wetness impregnation. In VOC oxidation it was found that $Pt/TiO_2 > Pd/TiO_2 \gg Rh/TiO_2 \approx Ir/TiO_2 \gg Au/TiO_2$. This suggests that investigations into the activity of different titania supports should focus on the most effective catalysts, i.e. Pt and Pd. More complex systems have also been envisaged whereby TiO_2 (40–64 wt%) and ZrO_2 (48–62 wt%) were inserted in SBA-15 mesostructured silica by chemical solution decomposition or hydrolysis of the corresponding alkoxides inside the host pores to obtain silica composites with crystalline anatase (TiO_2) and tetragonal (ZrO_2) phases [9]. When impregnated with 0.3 wt% Pt, these catalyst systems showed a 1.7–3 times greater activity in the combustion of ethyl acetate compared with Pt on bulk $Ti(Zr)O_2$ and 2 times greater activity than Pt/SBA-15 [9].

Although mesoporous supports offer an improvement over non-porous oxides, diffusion limitations can be minimised even further by interconnecting macropores with a micro(meso) pore system [10–12]. Narrow mesopore widths can increase contact between reactant and catalyst thus increasing the performance of the catalyst whereas the macrochannels act as conduits, accommodating bulky molecules and breaking them down before they enter the (micro)mesoporous network [13–16].

Macro-mesoporous ZrO_2, TiO_2 and ZrO_2–TiO_2 have been used as catalytic supports for Pd nanocatalyts in the total combustion of toluene and chlorobenzene [17–19]. These supports presented high surface areas with the porosity preserved after calcination at 400 °C for TiO_2 and ZrO_2–TiO_2 but not for ZrO_2. Pd/meso-macroporous TiO_2 presented the highest catalytic potential as it had the lowest toluene adsorption enthalpy, low coke content post-test and the PdO particles were easily reducible [17]. It was also found that the activity of Pd/meso-macroporous TiO_2 was superior to that of Pd/meso-macroporous ZrO_2 in the oxidation of chlorobenzene, most likely due to the reducibility of TiO_2 compared to ZrO_2 as this increases oxygen mobility across the support [19]. Pt nanoparticles have also been dispersed in hierarchically porous SiO_2 or SiO_2–TiO_2 matrices and investigated for the total oxidation of propene [20]. Light-off temperatures were lower than 110 °C at a 1.7 wt% Pt loading and due to the structuration of the support, thermal growth of the nanoparticles was hindered.

There is a limit to the improvements in light-off temperatures that can be achieved through structural and morphological tailoring of a primary oxide support. However by tweaking the chemical composition one can also boost the overall activity of classic systems, such as by doping a support with low levels of another catalytically active element or having a bi-phasic support in which a minor phase is supported upon the dominant phase prior to adsorption of a noble metal. One potential option is niobium, whose compounds are known to promote catalytic reactions [21–25]. Studies have been carried out into supported niobium oxides (on silica, aluminia, titania and zirconia etc.), as their catalytic activity can differ from bulk niobium oxide [26–28]. Dependent on surface coverage, the co-ordination of niobia can vary, with 4-fold coordinated NbO_4 species at low coverage, 5-fold NbO_5 for intermediate coverage and 6-fold NbO_6 at high coverage [21]. When niobia forms a surface layer over another support material it is quite stable owing to a strong niobium oxide-support interaction [29].

The benefits of niobium as a catalytic promoter lie in its inherent properties, for example it is a solid acid catalyst [21]. Hydrated Nb_2O_5 possesses an unusually high surface acidity and can increase activity in acid catalysed reactions [23]. Additionally, niobium can adopt variable oxidation states, unlike aluminium and silicon, which is useful for redox processes [30]. A principle application of niobium containing catalytic systems is in oxidation catalysis [21 and refs. therein].

The use of niobium doped titania has been reported in applications such as battery materials [31], photocatalysis [32–34] and gas sensing [35]. It would therefore seem logical to combine the redox properties of Nb with that of a hierarchically structured titiania support, which has already been proven in previous studies to improve activity [17–20], to design advanced catalysts via chemical doping. The aim of this study therefore was to introduce small amounts of a catalytic promoter, niobium, into micro(meso) macroporous titania to improve the efficiency of the catalyst system. The elaboration of state-of-the-art catalytic systems was achieved via the impregnation of noble metals (Pd, Pt) onto these supports and the performance of the systems was examined in terms of the total oxidation of several model pollutants (viz. butan-1-ol and toluene). Such molecules were chosen to represent both oxygenated and aromatic molecules typically found in industrial flue gases and which present a hazard to human health.

2. Materials and methods

2.1. Preparation of state-of-the-art Pd or Pt/Nb–TiO_2 catalysts

2.1.1. Preparation of hierarchically porous Nb–TiO_2 supports

Hierarchically porous Nb–TiO_2 supports were synthesised using the concept of auto-formation, without the need for an external templating agent [16,36]. In total three different niobium doping amounts were realised, 1, 3 and 5 at% Nb with respect to Ti. A basic solution (pH 12) was prepared from ammonium hydroxide and placed into a shallow dish with a large surface area. Stoichiometric amounts of $Ti(O^iPr)_4$ (Aldrich, ≥97.0%) and $Nb(OEt)_5$ (Aldrich, 99.95%) were thoroughly premixed prior to being added dropwise to the basic solution. Eventually the solution and the precipitate were transferred to a polypropylene autoclave and heated hydrothermally to 80 °C for 24 h. The autoclave was then removed to ambient temperature to cool and the product filtered and washed. The Nb–TiO_2 supports were then dried at 60 °C in air overnight. The supports were finally calcined at 400 °C for 4 h with a ramp rate of 1 min^{-1} prior to catalyst preparation.

2.1.2. Elaboration of state-of-the-art Pd and Pt supported catalysts

Pd and Pt catalysts supported by hierarchically porous Nb–TiO_2 materials were prepared using the aqueous impregnation method. A pre-determined amount of $Pd(NO_3)_2$ (Alfa Aesar, 99.9%) or $Pt(NH_3)_4(NO_3)_2$ (Aldrich, ≥50.0% Pt basis) solution was mixed with the support for 30 min such that the target impregnation was 0.5 wt% Pd or Pt respectively. The water was then removed by rotovaporation and the sample calcined under air (2 L h^{-1}) at 400 °C for

4 h with a ramp rate of 1° min^{-1}. Prior to catalytic testing with Pd samples a known quantity of sample was reduced under flowing 5% hydrogen (2 L h^{-1}) mixed with Argon at 200 °C for 2 h, where as for Pt samples a pre-treatment under air at 400 °C was conducted.

2.2. Characterisation techniques

Textural properties of the materials were analysed via adsorption–desorption of nitrogen at −196 °C with prior outgassing to ~10^{-4} bar. Low-angle and wide angle powder X-ray diffraction (PXRD) datasets were collected on a PANalytical X'pert PRO and a Bruker D8 Advance (using a LynxEye detector) diffractometer with Cu Kα radiation respectively. A Hitachi S-4800 scanning electron microscope (SEM) was employed to observe the morphology of the samples and to carry out elemental analysis via energy dispersive X-ray spectroscopy (EDX). Transmission electron microscopy (TEM) was performed with a Philips Tecnai 10 with an accelerating voltage of 80 kV to observe support material bound in resin and cross-sectioned using an ultramicrotome. X-ray photoelectron spectroscopy was carried out using a surface science SSX-100 with monochromated Al Kα radiation at 1486.6 eV and 35° incidence angle.

(Sub-ambient) temperature programmed reduction (TPR) profiles were recorded using an Altamira AMI-200 apparatus. Pt impregnated samples were heated from room temperature up to 900 °C, whereas Pd impregnated samples were heated from −40 up to 500 °C, at a heating rate of 5 °C min^{-1} in a flow of 5% H_2/Ar (30 mL min^{-1}) and hydrogen consumption was monitored and integrated using thermal conductivity (TC) detection over the whole temperature range.

Finally, the mass of Pd and Pt in each sample was quantified using inductively coupled plasma-optical emission spectroscopy (ICP-OES).

2.3. Adsorption isotherms

Adsorption isotherms of chosen model pollutants (toluene and butan-1-ol) were measured at 303 K using a BELSORP-max automatic manometric sorption analyser (Bel Japan, Inc.).

Prior to adsorption experiments, the samples (~50 mg) were outgassed under secondary vacuum (10^{-5} mbar) and heated to various temperatures for 12 h. The final outgassing temperature was 110 °C. The adsorbents were placed in an adsorption chamber and the adsorbates were dosed. The pressure change was monitored and the adsorbed amount was calculated by a mass balance on the gas phase before and after adsorption when the equilibrium was reached (pressure variation lower than 0.2% for 1500 s).

2.4. Catalytic testing methodology

The model pollutants toluene and butan-1-ol were chosen to represent aromatic and oxygenated VOCs respectively. In a typical catalytic test the complete oxidation of one of these pollutants was performed over 100 mg of each catalytic system described in 2.1.2 in a conventional fixed bed reactor with a temperature rise of 1 °C min^{-1}. The flow of VOC was set at 1000 ppm in a flow of air: (total flow of 100 mL min^{-1}). The products formed during combustion were analysed and quantified via gas chromatography using a CP-4900 microGC (Varian) with injections taken every 3 min. From these measurements conversion graphs were constructed to determine the temperature at which a 50% conversion had taken place, which was then compared to a series of previously published hierarchically porous $xTiO_2$–$yZrO_2$ catalyst supports with identical catalyst loadings.

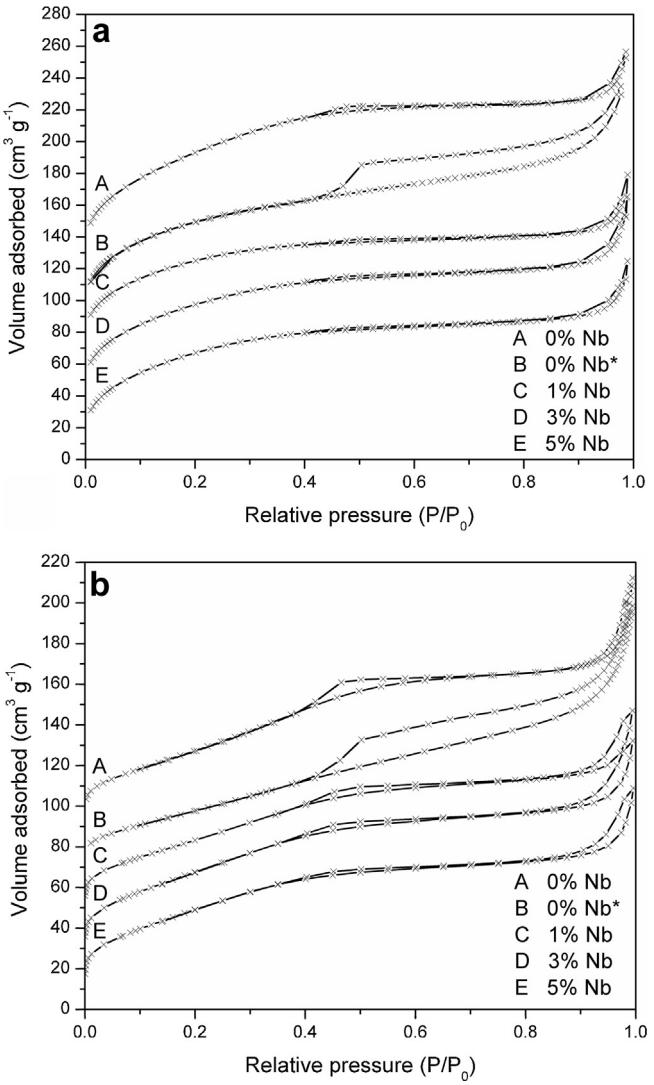

Fig. 1. Nitrogen adsorption–desorption isotherms as calculated via the BJH method (a) before calcination [isotherms: 0% Nb, 0% Nb*, 1% Nb and 5% Nb offset by +70, +40, +35 and −30 cm^3 g^{-1} for clarity] and (b) after calcination of hierarchically porous Nb–TiO_2 supports [isotherms: 0% Nb, 0% Nb*, 1% Nb and 3% Nb offset by +80, +60, +40 and +20 cm^3 g^{-1} for clarity]; 0% Nb* denotes sample synthesised in a micellar solution of Brij 56.

3. Results

3.1. Characterisation of hierarchically porous Nb–TiO_2 supports

3.1.1. Textural properties of Nb–TiO_2 supports

Textural characterisations of the uncalcined supports have revealed information about the hierarchical porosity of the supports. Fig. 1a shows the N_2 sorption isotherms of the three Nb doped supports, all of which have a strong tendency to type I isotherms, indicative of microporous materials, however the presence of a small H4 hysteresis suggests the presence of narrow slitlike mesopores. Before calcination each sample has a fairly high BET surface area, with similar values obtained for each sample (Table 1). As the level of Nb doping increases from 1% there is a slight increase in surface area before calcination (S_{BET} 3%Nb > 5%Nb > 1%Nb), though after calcination 5% Nb and 3% Nb are inversed with S_{BET} 5%Nb > 3%Nb > 1%Nb, however as the S_{BET} of 3 and 5% Nb is within a difference of 5 m^2 g^{-1} of each other, this is not significant enough to state that the level of Nb doping changes the surface area of the supports. The information elucidated

Table 1
Textural properties of hierarchically porous Nb–TiO_2 supports before and after calcination.

Nb (%)	S_{BET} ($m^2\ g^{-1}$)	S_{BET}[c] ($m^2\ g^{-1}$)	S_{micro} ($m^2\ g^{-1}$)	V_{micro} ($cm^3\ g^{-1}$)	d_{HK} (nm)
0[a]	432	177	80.1	0.036	1.54
0[b]	346	140	90.9	0.041	2.4
1	312	160	81.7	0.037	1.52
3	340	179	132	0.061	1.37
5	337	183	156	0.073	0.94

BET = Brunauer–Emett–Teller Theory.
HK = Horvath–Kawazoe Theory.
[a] Sample synthesised without templating agent.
[b] Sample synthesised in a micellar solution of Brij 56.
[c] After calcination.

suggests there is a minimal contribution to the overall porous volume from the micropores, yet a significant contribution to the surface area. With increasing niobium content there is an increase in microporous surface area and volume yet a decrease in micropore size. For comparison two pure titania samples were synthesised, one in the presence of a non-ionic surfactant, Brij 56 (isotherm B, Fig. 1a), and one without (isotherm A, Fig. 1a). When surfactant is employed there is evidence of an increase in pore size towards the meso-scale as the isotherm has similarities to that of a IUPAC type IV isotherm (Fig. 1aB). However in the absence of surfactant the TiO_2 isotherm follows that of the Nb doped supports (Fig. 1aA), albeit with a larger BET surface area.

After calcination at 400 °C there is a 50% reduction in BET surface area and an increase in mesoporosity. There is no longer evidence of micropores, suggesting a large-scale disappearance of these micropores [37]. Finally the strong N_2 uptake and more evident H4 type hysteresis loop at higher relative pressures reveal that the mesopores remain intact after calcination.

The scanning electron microscopy (SEM) images in Fig. 2 clearly show the macroporosity of the samples, with the porous channels running quasi-parallel to each other and radially to the surface of the sample. The pore channels appear to get larger as they descend away from the surface with the apertures at the surface around 1 μm in diameter. The transmission electron microscopy images obtained on cross-sections of the samples gives a pore size of around 5 μm (Fig. 3). The higher magnification SEM images reveal that the macropores are comprised of aggregations of nanoparticulate matter, which is confirmed by TEM. The TEM images also reveal macropore walls around 2–3 μm thick formed from the aggregation of nanoparticulate oxides and contained within these walls are interconnected wormlike channels contributing to the micro(meso)porosity of the sample. The combination of results obtained from N_2 adsorption–desorption, mercury intrusion (results in SI 1) and electron microscopy (SEM, TEM), confirms that the as-synthesised materials have a hierarchical porosity on the micro(meso)macro scale and that after calcination, the presence of mesopores is more established, which is critical to the performance of the support in catalysis.

Low angle powder X-ray diffraction (PXRD) analyses have revealed a broad peak between $1 < 2\theta < 3$ for the uncalcined supports confirming that these samples are porous (Fig. 4a). As this peak is not well defined it implies that the pore structure is disordered, in other words there is no long range ordering or orientation of the micro(meso)pores. A broad peak may also indicate that the pores are multimodal in size. One observation to be made is that the maximum of the broad peak shifts towards higher 2θ, suggesting that the average pore size decreases, with increasing niobium content. This would be in agreement with the micropore sizes obtained from applying Horvath–Kawazoe theory to the N_2 adsorption–desorption measurements (Table 1) [38].

3.1.2. Chemical composition and crystallography of Nb–TiO_2 supports

In this work the chemistry of alkoxides has been exploited in order to insert Nb ions into the framework of TiO_2 whilst preserving a porous network. Using a traditional solid state route based on primary oxides as reactants, the calcinations temperature to achieve Nb insertion is too high to retain a porous scaffold.

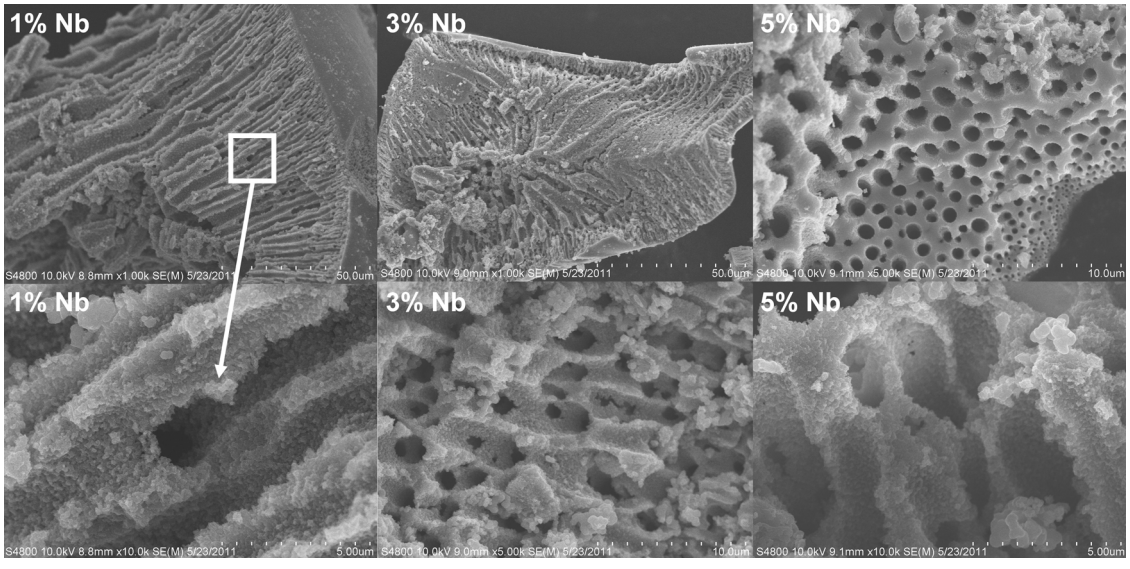

Fig. 2. Various scanning electron microscopy images of hierarchically porous Nb–TiO_2 supports before calcination.

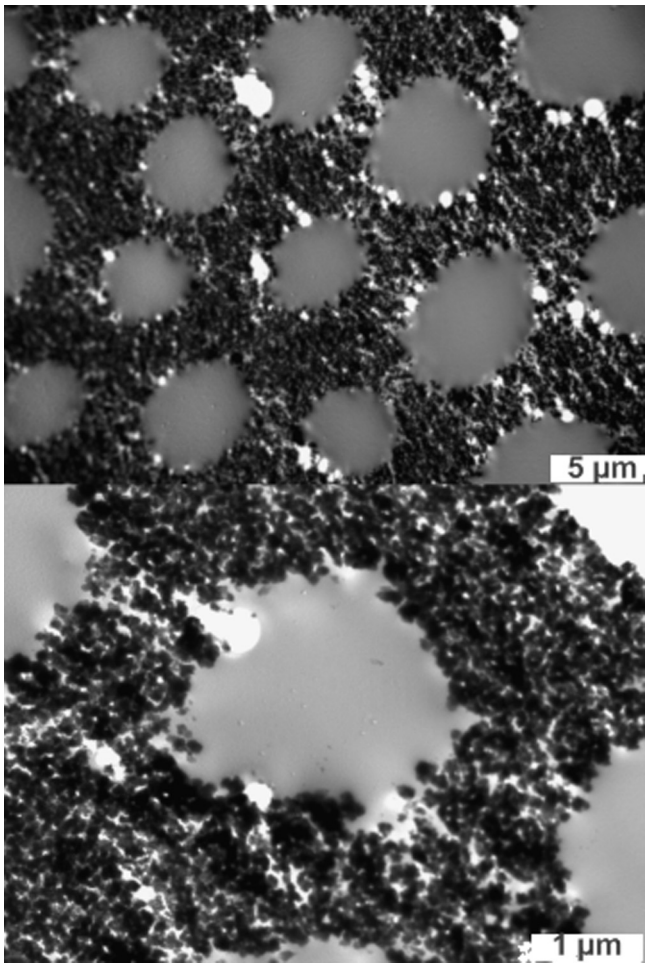

Fig. 3. Transmission electron microscopy cross-section images of hierarchically porous Nb–TiO_2 supports before calcination, where the scale bars represent 5 μm (upper) and 1 μm (lower).

However in this work the formation of Ti—O—Nb bonds is achieved at room temperature during the co-precipitation of a homogeneous mix of alkoxides of a pre-determined stoichiometry. As the alkoxides are added to the aqueous media, they instantly hydrolyse forming hydroxyl groups which subsequently undergo condensation to form an oxide framework. During this process intermediate hydroxyl groups viz. Ti–OH and Nb–OH can thus react together resulting in a Ti–O–Nb connectivity prior to crystallisation at 400 °C.

The variable temperature PXRD data given in Fig. 4b is representative of all three samples, with the onset of the metastable anatase phase at 400 °C, the temperature at which catalyst elaboration occurs. The crystal radii of Nb^{5+} and Ti^{4+} when found in a 6-co-ordinate environment, 78 pm vs 74.5 pm (Shannon [39]), are very similar in size and thus it is possible that Nb^{5+} is incorporated within the anatase lattice on the same sites as Ti^{4+}. Furthermore no second phase such as Nb_2O_5 is detected in the wide angle PXRD profile.

Reitveld refinements have been carried out on the three doped Nb–TiO_2 samples, modelling the experimental PXRD results against an anatase phase found in the JCPDS database (File No. 75-2545) [40]. The statistics obtained from these results (not shown) reveal that the correlation between the experimental and the theoretical models is good, with minimal variation. This modelling has shown that there is a slight increase in lattice parameters and in the unit cell volume on increasing niobium content which would be consistent with the insertion of a slightly bigger cation onto the Ti^{4+} site.

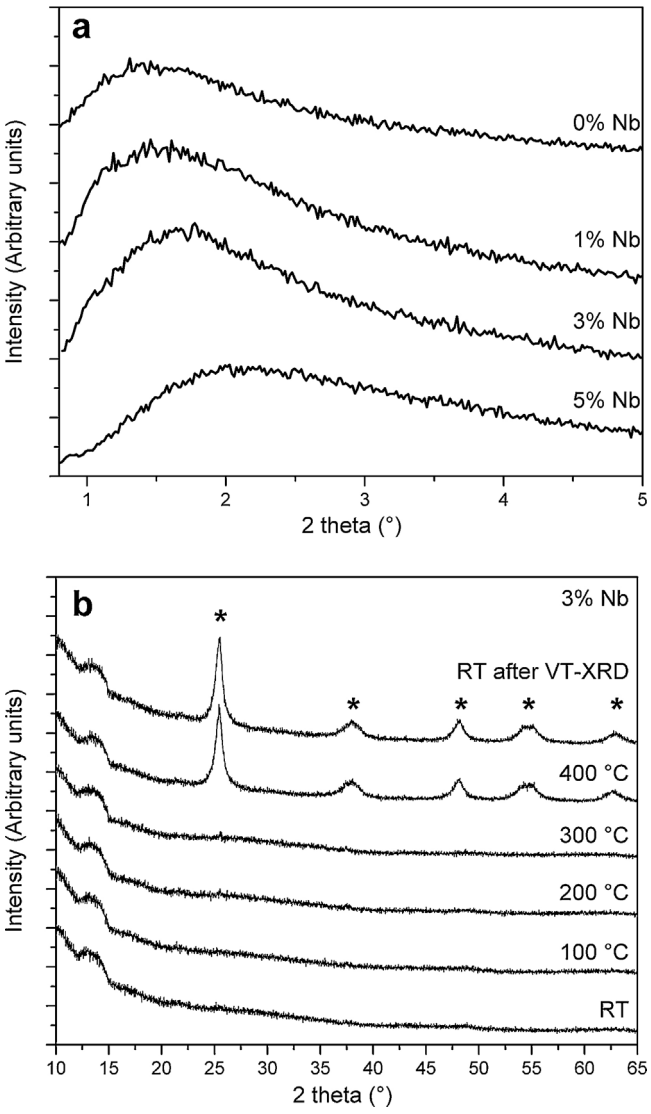

Fig. 4. Powder X-ray diffraction datasets for hierarchically porous Nb–TiO_2 supports where (a) corresponds to low-angle measurements and (b) variable temperature wide angle measurements for 3% Nb, where * indicates the peaks indexed against JCPDS 75-2545, TiO_2 anatase phase.

Carotta et al. have suggested the inclusion of Nb within titania hinders both grain growth and phase transition to the thermodynamically stable rutile phase [41], the latter arising from a reduction in oxygen vacancies to counterbalance the increase in cationic charge. Niobium doping appeared to increase the thermal stability of the anatase phase, increasing the temperature at which the sintering of particles occurred. This was confirmed by the increased surface area of an Nb doped titania over titania which had both been calcined at 700 °C until a constant surface area was obtained. Fig. 5 shows that there is a slight reduction in crystallite size on Nb incorporation. The increase in cationic charge on Nb^{5+} over Ti^{4+} may reduce the M—O—M bond lengths within the crystal, which could account for the delay in phase transformation to the thermodynamically stable rutile phase.

Field mapping studies (SI 2) have revealed that niobium is located throughout each of the supports, suggesting a homogeneous incorporation of the doping element into the TiO_2 based materials. The accompanying EDX results (Table 2) have shown a level of doping close to the targeted ratio values and are in agreement with results obtained from another surface technique, X-ray photoelectron spectroscopy (XPS) [37]. This technique revealed

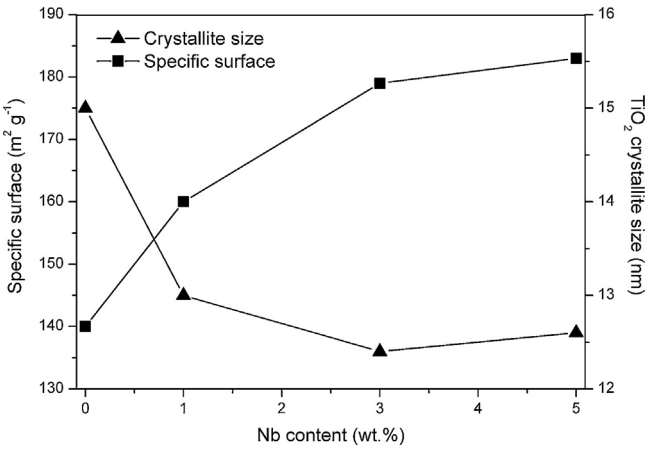

Fig. 5. Graph depicting variation in specific surface (■) and crystallite size (▲) of various hierarchically porous Nb–TiO_2 supports after calcination in relation to niobium content.

Table 2
TiNb via energy dispersive X-ray spectroscopy of hierarchically porous Nb–TiO_2 supports; each entry is an average of the results from three zones of a sample.

Sample name element	1% Nb		3% Nb		5% Nb	
	at%	Mass%	at%	Mass%	at%	Mass%
Ti	99.1	98.2	97.4	95.1	94.6	90.0
Nb	0.9	1.8	2.6	4.9	5.4	10.0

that niobium is indeed in the +5 oxidation state, with no indication of Nb^{4+} species (Fig. 6). The high resolution Nb 3*d* spectrum reveals a doublet with the Nb $3d_{5/2}$ peak centred around 207.9 eV and Nb $3d_{3/2}$ at 210.7 eV with a spin orbit coupling of 2.8 eV which is in accordance with results obtained for Nb doped TiO_2 [31,42], with a study by Morris et al. [43] showing that at low level Nb doping the Nb 3*d* doublet corresponds to that of Nb_2O_5 implying that the substitutional Nb is incorporated into the lattice in the +5 oxidation state. As stated in the literature when Nb^{5+} is inserted into TiO_2, it creates either one Ti site vacancy per 4 Nb^{5+}, it reduces one Ti atom from a +4 oxidation state to +3, or it evokes an oxygen interstitial per two Nb^{5+} cations [44]. In this work the high resolution Ti 2*p* spectra reveal a satellite peak around 14 eV from the main peak located at 459.6 eV which when coupled with the 2*p* doublet separation of 5.8 eV is indicative of Ti^{4+} in TiO_2 [45]. There is also no evidence of an additional peak characteristic of Ti^{3+}, thus confirming there is no reduction amongst the Ti species to compensate for the inclusion of Nb^{5+} ions. This is also consistent with the white colouration of the samples as even a slight reduction in titanium ($TiO_{2-\delta}$) results in a colour change from that of TiO_2 owing to charge transfer effects between the Ti^{3+}/Ti^{4+} couple. Finally the shoulder in the O 1*s* peak is a result of terminal hydroxyl groups and adsorbed oxygen on the surface of the Nb doped TiO_2. The comparison of XPS and ICP results showed that the ratios of Nb/Ti at the surface by XPS (0.0079, 0.0235 and 0.0414 for 1, 3 and 5% doping, respectively) and in the bluk by ICP (0.0093, 0.0295 and 0.0519 for 1, 3 and 5% doping respectively) are very similar, suggesting that Nb ions are very homogeneously dispersed in the crystal lattice of

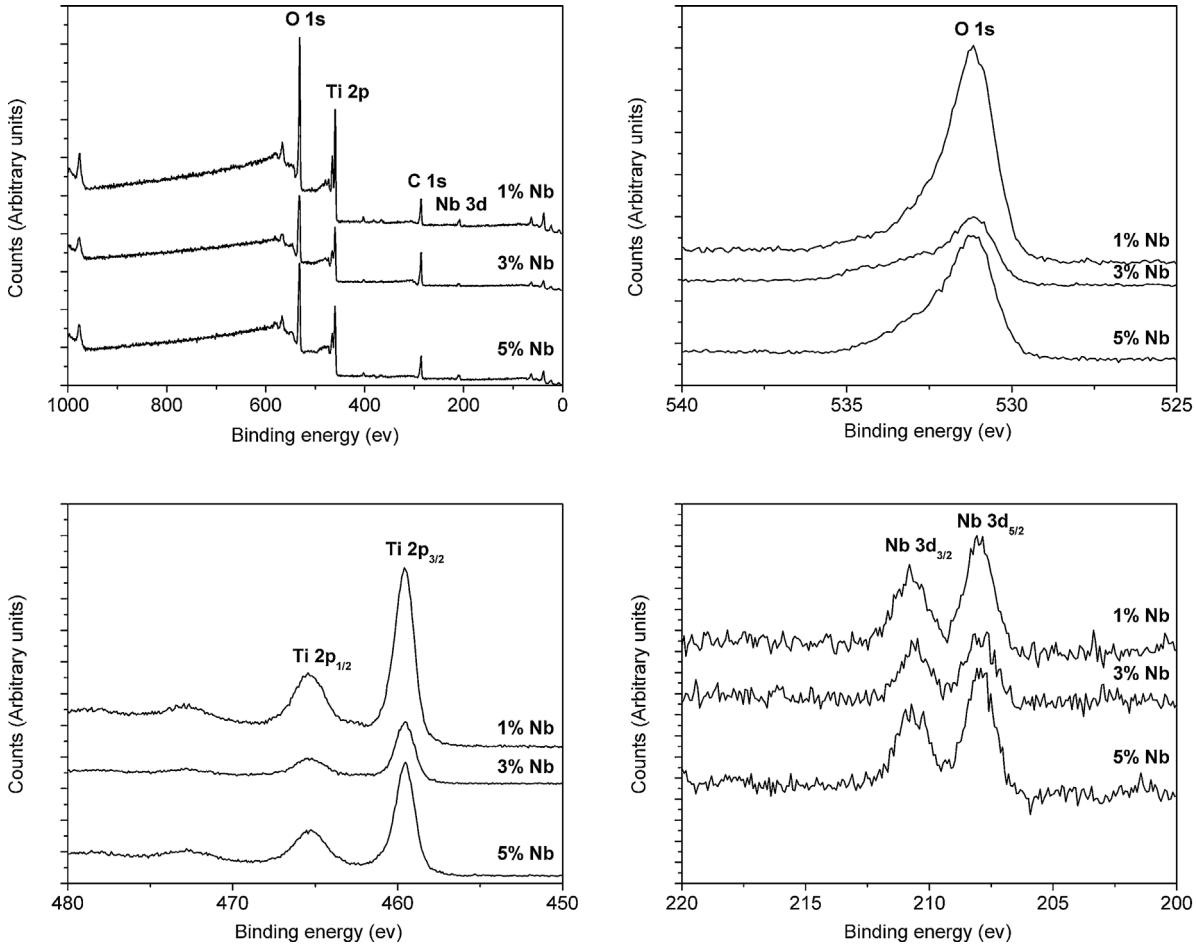

Fig. 6. A wide range X-ray photoelectron spectrum of the hierarchically porous Nb–TiO_2 supports, before calcination, with high resolution scans of the most intense peaks of each element contained within the samples.

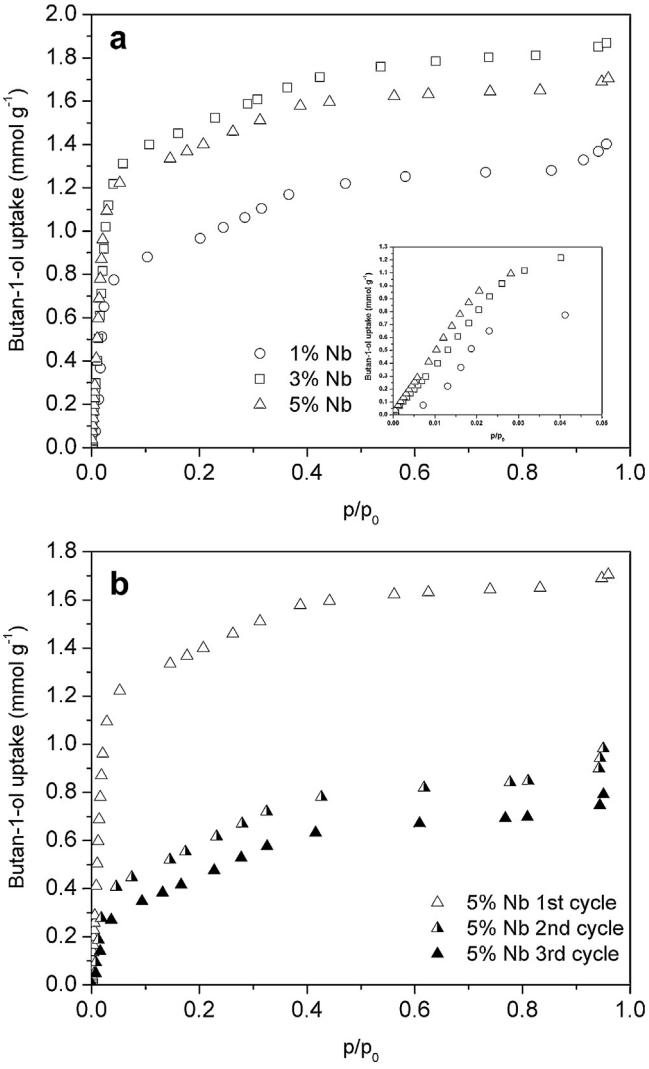

Fig. 7. Butan-1-ol adsorption isotherms obtained for (a) pre-calcined 1, 3 and 5% Nb–TiO_2 hierarchically porous supports and (b) first and second cycle butan-1-ol adsorption isotherms obtained using 5% Nb–TiO_2 before calcination, and third cycle obtained using 5% Nb–TiO_2 after calcination at 400 °C. Outgassing at 110 °C was performed each time prior to measurements.

TiO_2. Furthermore, our recent TOF-SIMS study which will be published elsewhere demonstrated that Nb ions are well incorporated in the TiO_2 crystal lattice since Nb ions are in strong interaction with Ti ions.

3.2. Adsorption capacities of hierarchically porous Nb–TiO_2

Fig. 7a shows the butan-1-ol adsorption isotherms at 30 °C obtained for the three doped supports, all of which have the same isotherm shape. Interestingly, there are several distinct steps in the isotherms. The butan-1-ol adsorption isotherms show clear steps because of the presence of energetically different sites. High butan-1-ol uptake at low pressure ($p/p_0 < 0.05$), arising from strong interactions, confirms that the support materials present significant microporosity before calcination. For p/p_0 from 0.05 to 0.4, adsorption occurs in the mesoporous spaces and pore surfaces of the materials. Furthermore, the isotherms show a plateau. At high pressure ($p/p_0 > 0.95$), capillary condensation occurs in the mesopores. Finally, the initial slope of the isotherms increases with an increase in niobium concentration within the structure. This is clearly a function of the microporous diameter; the diameter decreases with increasing niobium concentration in the sample (see d_{HK} values, Table 1).

The maximum adsorbed quantities of butan-1-ol at a relative pressure of 0.94 are 1.4, 1.8 and 1.7 mmol g^{-1} for 1%, 3% and 5% Nb respectively. These results are in relation with the specific area of the three samples (312 m^2 g^{-1}, 340 m^2 g^{-1}, 337 m^2 g^{-1}). The maximum uptake of each support depends directly on the adsorption capacity of the micropores within the supports, with the uptake within the mesopores being quasi-similar for the 3 samples (0.63, 0.69 and 0.68 mmol g^{-1} for 1%, 3% and 5% Nb respectively).

After the first butan-1-ol adsorption isotherms were established, each sample was outgassed at 110 °C under a secondary vacuum (same conditions as the initial outgassing procedure). The adsorption experiment was then re-run, with the results from 5% Nb–TiO_2 displayed in Fig. 7b representing the general observations for each sample (similar trends). The second butan-1-ol adsorption isotherm obtained for 5% Nb–TiO_2 shows a significant decrease in the maximum uptake. This comes from a substantial decrease in the microporous contribution to the total butan-1-ol uptake (63% lost). This implies that it is not possible to remove a large part of the adsorbed butan-1-ol from the micropores under the original outgassing conditions.

Finally, the samples were calcined at 400 °C (corresponding to the temperature of calcination during noble metal impregnation) and the adsorption experiment repeated for a third time. After calcination, the butan-1-ol isotherm for the 5% Nb–TiO_2 sample revealed a further considerable decrease in the maximum uptake (Fig. 7b). This decrease was larger than that observed in the second isotherm obtained after the first desorption of butan-1-ol. The butan-1-ol uptake in the microporous range decreases by 79%. As the N_2 isotherm at 77 K for low relative pressures has shown, a large part of the micropores collapse during calcination of the sample, the remaining BET surface area (160, 179 and 183 m^2 g^{-1} for 1%, 3% and 5% Nb respectively) comes essentially from the mesoporosity of the sample. Results on the adsorption of toluene followed an identical trend.

3.3. Hydrogen temperature programmed reduction of catalytic systems based on hierarchically porous Nb–TiO_2 supports

The hierarchically porous Nb–TiO_2 supports were impregnated with Pd and Pt noble metal nanoparticles. These materials have been analysed to see the effect of niobium doping on the activity of the whole system. The XRD measurements of as prepared and calcined catalysts with the impregnation of Pd and Pt showed no presence of a Pd or Pt lattice and no formation of big agglomerations of Pd or Pt atoms, indicative of very small particle size and a very good dispersion of Pd and Pt.

H_2-temperature programmed reduction (TPR) of the calcined supports before impregnation has shown that generally, the increasing presence of niobium delays the partial reduction of TiO_2 which occurs at elevated temperature (Fig. 8a). This can be seen in the peak found at 600 °C for unimpregnated and undoped TiO_2, which is shifted to slightly higher temperatures for the 3 and 5 at% Nb doped TiO_2. Conversely the impregnation of platinum favours the partial reduction of TiO_2 as can be seen by the broadening of the peak found in the upper datasets of Fig. 8b.

This improvement in reducibility of platinum impregnated samples can be explained by the hydrogen spillover effect on Pt^0 species formed at the beginning of the reduction experiment [46]. TPR analysis of the samples impregnated with palladium was carried out under sub-ambient conditions as the reduction of Pd occurs at much lower temperatures. Normally a well defined peak is seen at 0 °C, corresponding to the reduction of surface PdO species, as highlighted in the Pd/TiO_2 profile in Fig. 8c. This peak is absent in the Pd/Nb–TiO_2 samples. This indicates that Pd is already reduced,

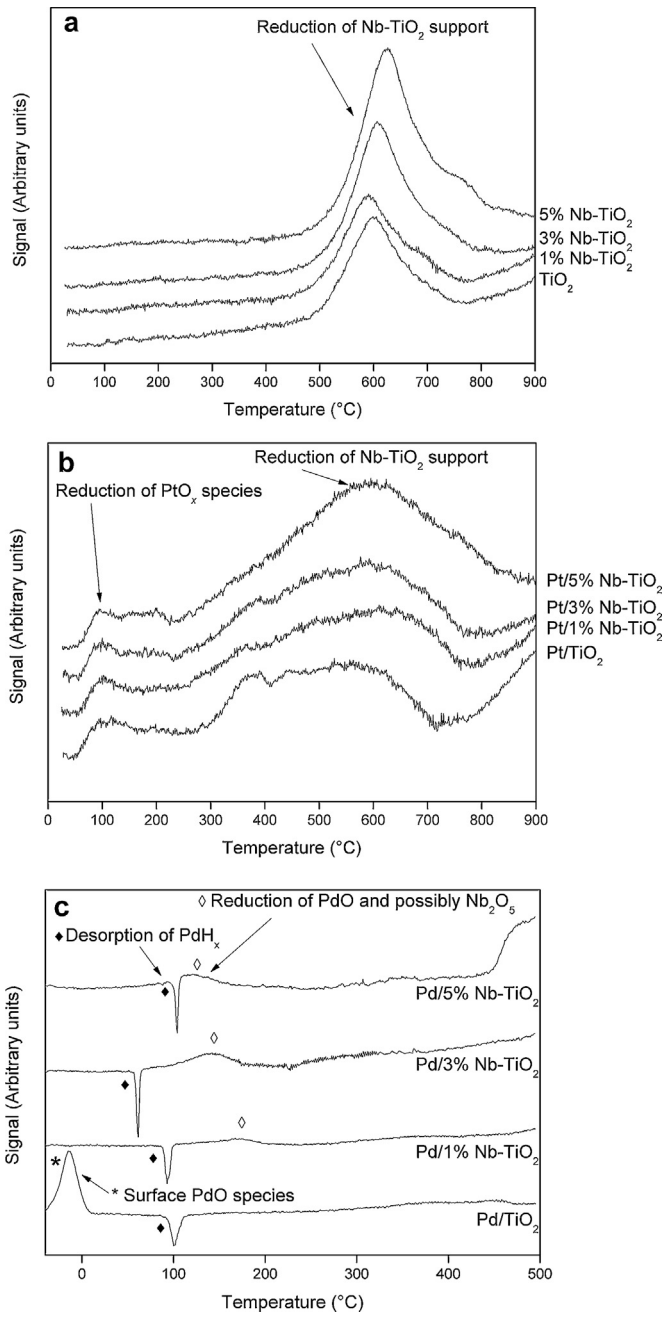

Fig. 8. H_2-temperature programmed reduction of (a) calcined Nb–TiO_2 in comparison to (b) Pt deposited on calcined Nb–TiO_2 and (c) Pd deposited on calcined Nb–TiO_2.

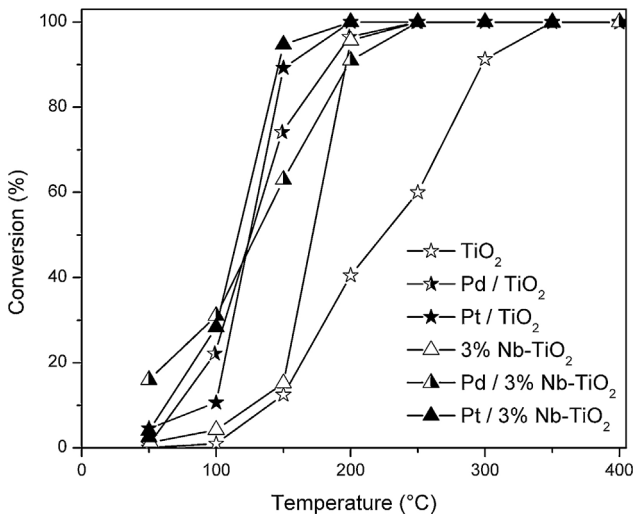

Fig. 9. Representative graphs showing the conversion of butan-1-ol with increasing temperature for TiO_2 alone, TiO_2 doped with 3 at% Nb and these supports impregnated with either Pd and Pt.

which is confirmed by the negative peak at 100 °C, attributable to the decomposition of palladium hydrides (PdH_x). The broad peak between 150 and 200 °C should correspond to the reduction of PdO species. These species can often be found in bulky Pd particles or stuck deep in the porous structure. However as the Pd is already predominately reduced, the profiles reveal that hydrogen consumption is higher than the theoretical consumption, indicating that Nb species could also be reduced. It has been reported in the literature that Nb is reduced at lower temperatures, between 100 °C and 200 °C, in the presence of Pd [47,48]. Tauster et al. [47] have revealed, though spectroscopy, the interactions that can exist between group VIII metal particles and the inorganic support they are dispersed upon. They explained how surface atoms can be reduced to form cations (for instance Nb^{5+} to Nb^{4+}) and in turn the additional electron can be transferred to the adsorbed species (such as Pd or Pt) hence reducing the noble metal adsorbate. This argument can be used to suggest that the absence of reduction peaks at low temperatures in the TPR curves and the decrease in temperature at which PdO is reduced is due to a possible interaction between Nb and Pd. Finally, the broad peak that starts at around 480 °C, most visible in Pd/5% Nb–TiO_2, is the onset of the reduction of the support itself, as seen in the Pt samples in Fig. 8b.

XPS analysis of the Pt $4f_{7/2}$ peak reveals that when doping with niobium there is a reduced platinum species (Pt^0) present alongside the Pt^{2+} species [37]. The presence of reduced platinum is a direct result of the Ti site vacancies created by the incorporation of Nb^{5+} species into the anatase framework as this changes the electron mobility of the solid, promoting Pt reduction.

3.4. Catalytic performance of M/Nb–TiO_2

3.4.1. Catalytic oxidation of butan-1-ol

In order to determine the role of niobium as a catalytic promoter, the support materials were tested in the absence of noble metals and compared to the activity of a hierarchically porous titania without niobium for the catalytic oxidation of butan-1-ol, a model oxygenated VOC.

Results on the total oxidation of butan-1-ol over hierarchically porous Nb–TiO_2 materials have shown that the presence of niobium within titania can substantially reduce the T_{50}, the temperature at which a 50% conversion has been achieved, by over 50 °C. Furthermore the T_{90} at 5% Nb doping decreased by over 100 °C thus indicating a sharp increase in activity of the support itself upon Nb loading. This increase in activity is also seen at low temperatures cf. T_{30} values. This may arise from a greater interaction between the adsorbate, in this case butan-1-ol, and the Nb^{5+} sites in the framework compared to the adsorbate–Ti^{4+} interaction. However in the absence of noble metals there is a lowering in selectivity towards CO_2 (target product) with a presence of CO in the off stream at 100% conversion for all samples (Figs. 9 and 10 and Table 3).

When impregnated with noble metals there is an improvement in catalytic performance (greater activity at lower temperatures) as well as in selectivity, judged by an increased CO_2 yield over CO, for all catalysts. At low reaction temperatures (<150 °C) the major secondary products during the oxidation are aldehydes (mainly butanal) and some CO as seen in Table 3. At higher reaction temperatures (>150 °C) full conversion is attained and the only detectable

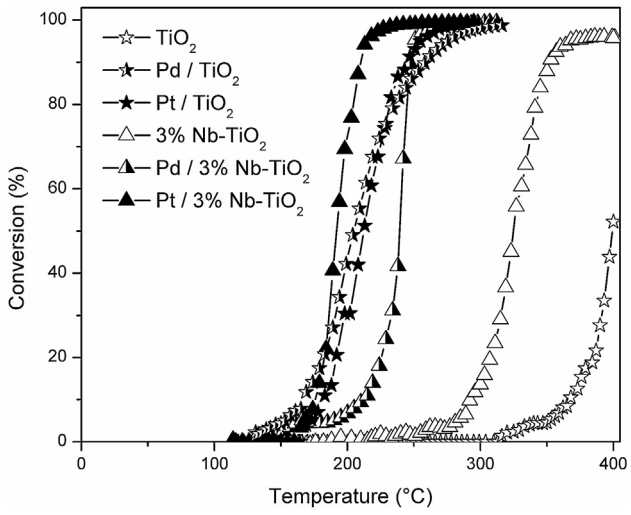

Fig. 10. Representative graphs showing the conversion of toluene with increasing temperature for TiO_2 alone, TiO_2 doped with 3 at% Nb and these supports impregnated with either Pd and Pt.

product is CO_2. The calculated activity at both reaction temperatures reveals that for Pt impregnated systems the Nb doped catalysts are substantially more active than the Nb-free sample, this is probably due to the modification of the platinum oxidation state by the addition of niobium [37]. There is also no CO formation at 150 °C for Nb doped Pt catalysts, unlike for pure titania, suggesting complete oxidation is more facilely achieved. These results clearly emphasise the role of a catalytic promoter, in this case Nb, within the catalytic system to decrease conversion temperatures and thereby reduce energetic costs.

Pd addition improves the catalytic performance at low oxidation temperature (50–100 °C), with T_{30} temperatures revealing a marginally better performing catalyst system than Pt loaded supports. Nevertheless the activity shown by these catalysts at temperatures in excess of 100 °C is lower than Pt impregnated samples. There is also little difference between the activities of Pd supported on TiO_2 or on Nb–TiO_2, with just a slight increase on Nb addition, suggesting the role of niobium is inconsequential for Pd catalysis.

There is no significant difference between the T_{50} of the platinum supported catalysts, however the Pt loading decreases slightly as niobium doping occurs so this will have a certain influence over the calculated T_{50} values. This is especially true for the undoped samples where Pt loading is higher. This increase in Pt would be enough to decrease the T_{50} value, bringing it into the same range as Nb doped samples. In essence this suggests that similar catalytic activities can be achieved using less Pt per gram of support simply by incorporating niobium, a relatively cheaper metal, into the support material. This therefore demonstrates the benefit of adding a catalytic promoter such as Nb into a known catalytic system.

3.4.2. Catalytic oxidation of toluene

Nb doped titania supports and their corresponding Pd and Pt loaded samples were tested in the oxidation of toluene, a model aromatic VOC, and resulting activities were compared with those of pure macro-mesoporous titania and its corresponding noble metal loaded catalysts.

Initial results showed a promoting effect of doping TiO_2 with Nb, as the activity of the support alone towards toluene oxidation increased on increasing Nb content. T_{50} values decreased by a minimum of 50 °C after Nb doping, with the lowest value corresponding to the highest Nb percentage (T_{50} = 322 °C). Activity was also increased at lower temperatures for higher Nb content, as seen by a shift in T_{30} values by almost 80 °C (*c.f.* 0% vs 5% Nb), confirming the role of Nb as a catalytic promoter. It was also noted that with pure titania, a 90% conversion of toluene was achieved above 400 °C, whereas after doping, 98% toluene conversion yields were obtained at temperatures around 370 °C, again demonstrating the promoting effect of Nb doping. Since PXRD, XPS, ICP and TOF-SIMS techniques confirmed the incorporation of Nb ions in the crystal lattice of TiO_2, the Nb promotion effect is not induced by a surface effect, but indeed a doping effect.

After loading noble metals (Pd and Pt) over pure and doped titania supports, results were different from what was expected. Doping with Nb improved the selectivity and activity whilst decreasing the T_{50} of Pt based systems, yet globally had less effect

Table 3
Catalytic activity in the total oxidation of butan-1-ol.

Catalyst	T_{30} (°C)	T_{50} (°C)	T_{90} (°C)	Wt (M%)	Temp (°C)	Activity[a] (h^{-1})	Yield (%)			
							CO_2	CO	Butanal	Butanol
TiO_2	182	225	298	N/A	150	N/A	0	0	25	88
					300	N/A	38	15	32	9
1%Nb–TiO_2	163	174	223	N/A	150	N/A	0.33	0.27	3.62	87.89
					300	N/A	69.95	8.10	0.00	0.00
3%Nb–TiO_2	160	174	196	N/A	150	N/A	0.00	0.00	4.05	84.80
					300	N/A	52.33	30.12	0.00	0.00
5%Nb–TiO_2	159	174	195	N/A	150	N/A	0.00	0.00	4.23	85.03
					300	N/A	81.27	2.56	0.03	0.00
Pd/TiO_2	106	125	184	0.40	150	19.9	4.8	0	18.3	25.9
					300	26.9	88.7	0	0	0
Pd/1%Nb–TiO_2	100	125	195	0.37	150	20.2	2.3	0.30	19.79	33.00
					300	30.1	85.0	0.30	0.00	0.00
Pd/3%Nb–TiO_2	98	128	198	0.40	150	17.8	2.3	0.1	17.55	37.00
					300	28.3	83.5	0.40	0.05	0.00
Pd/5%Nb–TiO_2	100	123	181	0.41	150	20.3	3.2	0.30	18.81	25.00
					300	27.1	80.6	0.20	0.00	0.00
Pt/TiO_2	112	124	154	0.36	150	48.9	5.76	11.40	0.06	10.76
					300	54.8	92.4	0.00	0.00	0.00
Pt/1%Nb–TiO_2	105	125	151	0.29	150	59.6	19.3	0.00	15.85	10.06
					300	66.2	99.1	0.00	0.00	0.00
Pt/3%Nb–TiO_2	102	125	147	0.26	150	70.9	70.2	0.00	15.37	5.25
					300	74.8	100	0.00	0.00	0.00
Pt/5%Nb–TiO_2	102	124	165	0.24	150	70.5	14.7	0.00	1.62	11.98
					300	80.0	93.5	0.00	0.00	0.04

[a] Activity was calculated in terms of mol n-butanol reacted over mol of noble metal M (Pd or Pt) per hour.

Table 4
Catalytic activity in the total oxidation of toluene.

Catalyst	T_{30} (°C)	T_{50} (°C)	T_{90} (°C)	Wt (%)	Temp (°C)	Activity[a] (h^{-1})	Yield (%)			
							CO_2	CO	Benzene	Toluene
TiO_2	392	397	–	N/A	150	N/A	0.00	0.00	0.00	94.45
					300	N/A	0.00	0.00	0.00	82.51
1%Nb–TiO_2	332	341	368	N/A	150	N/A	0.00	0.00	0.00	71.90
					300	N/A	6.49	12.96	0.00	47.58
3%Nb–TiO_2	316	325	351	N/A	150	N/A	0.09	0.00	0.00	101.09
					300	N/A	30.25	11.69	0.00	72.89
5%Nb–TiO_2	313	322	343	N/A	150	N/A	0.00	0.00	0.00	96.93
					300	N/A	30.25	10.69	0.00	67.45
Pd/TiO_2	191	206	260	0.40	150	1.3	5.46	0.00	0.11	82.19
					300	30.3	98.52	0.00	0.15	1.07
Pd/1%Nb–TiO_2	233	239	247	0.37	150	0.8	6.47	0.00	0.45	79.78
					300	40.8	102.22	0.00	0.17	0.20
Pd/3%Nb–TiO_2	233	239	247	0.40	150	0.1	4.61	0.00	0.22	79.37
					300	48.9	90.04	0.00	0.03	0.22
Pd/5%Nb–TiO_2	199	209	242	0.41	150	1.5	6.09	0.00	0.36	66.74
					300	42.9	100.00	0.00	0.27	1.02
Pt/TiO_2	199	212	245	0.36	150	0	0.00	0.00	0.00	96.95
					300	62.5	94.61	0.00	0.00	0.47
Pt/1%Nb–TiO_2	190	196	210	0.29	150	0	0.00	0.00	0.00	94.93
					300	91.6	98.50	0.00	0.00	0.23
Pt/3%Nb–TiO_2	186	192	210	0.26	150	0	0.00	0.00	0.00	99.43
					300	88.7	99.95	0.00	0.00	0.22
Pt/5%Nb–TiO_2	196	209	246	0.24	150	0	0.00	0.00	0.00	97.06
					300	97.5	95.92	0.00	0.00	0.35

[a] Activity was calculated in terms of mol toluene reacted over mol of metal (Pd or Pt) per hour.

on Pd based catalysts, with a fluctuation in T_{50} and no change in selectivity towards CO_2 at the temperatures examined. However the activity of Pd loaded samples did increase upon Nb addition, with Pd/5%Nb–TiO_2 being the best performing Pd Nb-doped catalyst, when considering both activity and selectivity. The T_{50} of Pd/TiO_2 and of Pd/5%Nb–TiO_2 are similar in value yet on observing the graph (see Table 4) one can see a shallower gradient; 90% conversion does not occur until around 260 °C, whereas the T_{90} at 5% niobium doping was 242 °C. One slight anomaly is that although the conversion of toluene is almost at 100% for Pd/3%Nb–TiO_2 the amount of CO_2 detected is around only 90% at 300 °C suggesting the formation of an intermediary degradation product that was not identified by GC prior to complete oxidation.

Pd/TiO_2 showed a slightly better performance at lower temperatures towards toluene oxidation than Pt/TiO_2 with lower T_{30} and T_{50} values, though by 300 °C the activity of the Pt system was superior to its Pd counterpart. Although the activity was increased in Pt samples upon Nb doping, this activity was irrespective of the amount of Nb incorporated, with Pt/5%Nb–TiO_2 > Pt/1%Nb–TiO_2 > Pt/3%Nb–TiO_2 in terms of best activity, with only a minor increase in selectivity on Nb doping.

Overall Pd/Nb doped systems started to be active in the degradation of toluene at lower temperatures than Pt/Nb doped systems, though yet again by 300 °C Pt systems showed greater activity. In addition niobium reduced the low temperature activity of Pd systems with an increase in T_{30} values, suggesting the catalytic promotion of oxidation reactions by niobia doping is a complex issue.

CO and benzene were the major by-products of the oxidation of toluene over pure supports (TiO_2 and *x*Nb–TiO_2). However, after noble metal loading, CO was not detected and limited yields of benzene were recorded. This proves the higher catalytic effect of the noble metal active phase loaded onto these oxide supports. Finally, a decrease in toluene yield for hierarchically structured TiO_2 support was noted between 150 and 300 °C (Table 4), in the absence of reaction products (CO_2, CO and benzene). This result might be correlated with an adsorption of toluene molecules onto this support.

3.5. Discussion

It is well known that the surface area of a catalytic system influences its activity. This has been demonstrated herein as increasing the amount of niobium within a sample has increased the surface area (cf. 1 wt% vs 3 or 5 wt% Nb) and concomitantly both the VOC adsorption capabilities of these supports and their catalytic activities have improved. Increases in the adsorption capability of a support means that VOC molecules can be in greater contact with the catalyst, promoting their oxidation to H_2O and O_2 and concurrently boosting the overall performance of a system.

However surface area alone does not govern activity. As is generally acknowledged the chemical composition of a catalytic support material plays a vital role both in terms of activity of the support and the widely reported metal oxide support–catalyst interactions [3,49–51], and thus its contributions to the performance of the whole system are non-negligible. The amount of Pt deposited onto pure titania was greater than that deposited onto Nb doped titania, suggesting that the presence of Nb impeded the deposition process. This could be due to localised increases in positive charge on the support surface for Nb doped supports, as XPS data on the support material has revealed that no reduction of either the titanium or niobium species occurs. However, owing to the increase in activity of Nb doped samples towards oxidation with, in effect, less Pt per gram of catalyst, the interaction between both Ti–Nb and Nb–Pt must in fact be beneficial. Conversely the amount of Pd deposited onto both doped and undoped supports was more or less constant. EDX data suggests that an atomic Ti:Nb ratio of more than 95:5 can be achieved for the uncalcined samples. One study on Nb doped thick titania films suggested that Nb atoms can be substitutionally inserted for Ti^{4+} into a bulk anatase TiO_2 structure for up to 20 at% Nb without any segregation of niobium oxides [41], however Arbiol et al. studied the effect of Nb doping on the anatase to rutile transition and found that the solubility limit of Nb in the anatase TiO_2 phase was potentially around 3–4 at% [52]. This may suggest that not all Nb in the 5 wt% Nb–TiO_2 is located within the framework after calcination due to the stress placed on the lattice on increasing cation radius. However the amount of any competing niobium oxide phases as a percentage of the total sample would be very

low, and thus most likely undetectable in the diffractograms presented herein. Nevertheless, if the anatase framework has reached Nb saturation, the excess Nb is still present in the bulk material as revealed by EDX values and could thus still play a catalytic role. This would therefore account for the increase in activity values of Pt/5 wt% Nb–TiO_2 compared to the values obtained for lower Nb doping levels. What would be interesting to know is the isolation of niobium species within each system; with how much regularity are they substituted into the Ti–O–Ti framework? Although field mapping shows a homogenous distribution on the submicron scale, it tells us little about the distribution on the atomic scale. To know this might provide more insight into the mechanisms of the catalysed reaction that are occurring. Furthermore niobium is much less easily reduced than the more readily reducible group V_b element vanadium. As the boost in catalytic performance is due to redox effects between the doping element and the TiO_2 network, work has commenced on the substitution of Ti^{4+} for V^{5+} in the anatase framework of a hierarchically porous titania to see if this can improve the support–metal interaction further still.

It has been reported that small amounts of niobium oxide species added to a mixed oxide catalyst can play a promoting role [22]. Niobia can favour an ideal Pd^0/Pd^{2+} surface ratio in Pd/Al_2O_3 owing to the presence of NbO_x polymeric species near the monolayer [53]. Furthermore Pd loaded titania is widely known as a powerful catalyst, yet its activity does not last long as the Pd species tends to remain as Pd^{2+}. TPR studies presented here have shown that on increasing niobium content there is an improvement in reducibility of the platinum species with a slight shift to lower temperature. This may partially explain the improvement in low temperature activity of the Pt/Nb–TiO_2 systems over undoped Pt/TiO_2 in the oxidation reaction of butan-1-ol and toluene (cf. T_{30} values). A similar trend is observed for PdO species, which in general reduce at lower temperatures on increasing niobium content, except for high Nb content (5 wt%).

Researchers have found that in addition to doping the support (V, Nb etc.) other interactions can be introduced via the use of bimetallic catalysts (incorporation of Au say). This can result in electron transfers which reduce the Pd species and consequently stabilise the catalysts for longer. However, XPS analyses reveal that despite the addition of Nb into the titania structure, the oxidation state of palladium remains the same (2+) [37]. This might go some way to explain the poorer performance of Pd loaded Nb–TiO_2 in comparison to Pt loaded supports. The presentation of two different noble metals herein can be justified by explaining how attention also needs to be paid to the individual interactions present in each system, and that whilst excellent improvements are seen for Pt impregnated systems, these improvements are not as remarkable for Pd systems and as such other catalytic promoters or the use of bimetallic catalysts could be more interesting.

4. Conclusion

These results have shown the possibility of integrating Nb^{5+} ions onto the octahedral sites of Ti^{4+} within an anatase framework, owing to the similar crystal radii of both species, whilst retaining the morphological properties of hierarchically porous titania, established through a self-formation synthetic procedure. Hierarchical porosity has previously been shown to overcome limitations such as diffusion and pore accessibility within catalytic systems. Catalytic testing has shown how the use of a dopant such as niobium can play the role of promoter stemming from a strong metal-support interaction, which is especially marked in platinum containing catalytic systems. This was revealed by an increase in activity and CO_2 selectivity in the oxidation of butan-1-ol and toluene, model molecules for oxygenated and aliphatic VOCs, coupled with a decrease in T_{50} values compared to undoped supports with similar morphologies. This promoting effect was also observed to some extent in palladium samples at higher temperatures, with increasing niobium content boosting activity and selectivity. However the Pd catalytic system without niobium was better than the doped systems. In summary the benefit of incorporating Nb into the support matrix was best observed in the oxidation of toluene, where the temperature at which complete conversion was achieved (in the absence of noble metals) was reduced by around 80 °C for 5%Nb compared to undoped TiO_2.

Acknowledgements

This work was supported through a European Union project, REDUGAZ, funded by the Interreg IV France-Wallonie-Flandre programme. The French authors also thank the Région Nord Pas de Calais and the CNRS for an IRENI research grant and the Belgian authors also thank Walloon Region for financial support. The funding bodies had no influence in the scientific content of this manuscript. The authors are grateful for the technical assistance of Dr Ludovic Avril (XPS guidance) and Dr Dorothée Dewaele and all the CCM team (Pd) and the Service Central d'Analyse CNRS (Pt) for elemental analysis measurements.

Appendix A. Supplementary data

Supplementary data associated with this article can be found, in the online version, at http://dx.doi.org/10.1016/j.apcatb.2013.05.009.

References

[1] A.O. Malley, B.K. Hodnett, Catalysis Today 54 (1999) 31–38.
[2] C.P. Hubbard, K. Otto, H.S. Gandhi, K.Y.S. Ng, Journal of Catalysis 139 (1993) 268–276.
[3] K. Okumura, T. Kobayashi, H. Tanaka, M. Niwa, Applied Catalysis B 44 (2003) 325–331.
[4] J.R. González-Velasco, A. Aranzabal, J.I. Gutiérrez-Ortiz, R. López-Fonseca, M.A. Gutiérrez-Ortiz, Applied Catalysis B: Environmental 19 (1998) 189–197.
[5] R. Spinicci, A. Tofanari, M. Faticanti, I. Pettiti, P. Porta, Journal of Molecular Catalysis A: Chemical 176 (2001) 247–252.
[6] J.C.-S. Wu, Z.-A. Lin, F.-M. Tsai, J.-W. Pan, Catalysis Today 63 (2000) 419–426.
[7] H. Huang, D.Y.C. Leung, ACS Catalysis 1 (2011) 348–354.
[8] V.P. Santos, S.A.C. Carabineiro, P.B. Tavares, M.F.R. Pereira, J.J.M. Órfão, J.L. Figueiredo, Applied Catalysis B: Environmental 99 (2010) 198–205.
[9] X. Wang, M.V. Landau, H. Rotter, L. Vradman, A. Wolfson, A. Erenburg, Journal of Catalysis 222 (2004) 565–571.
[10] J.L. Blin, A. Léonard, Z.-Y. Yuan, L. Gigot, A. Vantomme, A.K. Cheetham, B.L. Su, Angewandte Chemie International Edition 42 (2003) 2872–2875.
[11] Z.-Y. Yuan, T.-Z. Ren, B.L. Su, Advanced Materials 15 (2003) 1462–1465.
[12] Z.-Y. Yuan, A. Vantomme, A. Léonard, B.L. Su, Chemical Communications (2003) 1558–1559.
[13] A. Vantomme, Z.-Y. Yuan, B.L. Su, New Journal of Chemistry 28 (2004) 1083–1085.
[14] Z.-Y. Yuan, T.-Z. Ren, A. Vantomme, B.L. Su, Chemistry of Materials 16 (2004) 5096–5106.
[15] Z.-Y. Yuan, B.L. Su, Journal of Materials Chemistry 16 (2006) 663–677.
[16] A. Vantomme, A. Léonard, Z.-Y. Yuan, B.L. Su, Colloid Surface A 300 (2007) 70–78.
[17] H.L. Tidahy, S. Siffert, J.-F. Lamonier, E.A. Zhilinskaya, A. Aboukaïs, Z.-Y. Yuan, A. Vantomme, B.L. Su, X. Canet, G. de Weireld, M. Frère, T.B. N'Guyen, J.M. Giraudon, G. Leclercq, Applied Catalysis A 310 (2006) 61–69.
[18] H.L. Tidahy, S. Siffert, J.-F. Lamonier, E.A. Zhilinskaya, A. Aboukaïs, Z.-Y. Yuan, A. Vantomme, B.L. Su, X. Canet, G. de Weireld, M. Frère, Studies in Surface Science and Catalysis 160 (2007) 201–208.
[19] J.M. Giraudon, T.B. N'Guyen, G. Leclercq, S. Siffert, J.-F. Lamonier, A. Aboukaïs, A. Vantomme, B.L. Su, Catalysis Today 137 (2008) 379–384.
[20] C. Yacou, A. Ayral, A. Giroir-Fendler, A. Baylet, A. Julbe, Catalysis Today 156 (2010) 216–222.
[21] I. Nowak, M. Ziolek, Chemical Reviews 99 (1999) 3603–3624.
[22] M. Ziolek, Catalysis Today 78 (2003) 47–64.
[23] T. Ushikubo, Catalysis Today 57 (2000) 331–338.
[24] M.O. Guerrero-Pérez, M.A. Banãres, Catalysis Today 142 (2009) 245–251.
[25] T. Beutel, V. Siborov, B. Tesche, H. Knözinger, Journal of Catalysis 167 (1997) 379–390.
[26] J.-M. Jehng, I.E. Wachs, Journal of Molecular Catalysis 67 (1991) 369–387.

[27] H. Yoshida, T. Tanaka, T. Yoshida, T. Funabiki, S. Yoshida, Catalysis Today 28 (1996) 79–89.
[28] R.M. Pittman, A.T. Bell, Catalysis Letters 24 (1994) 1–13.
[29] G. Deo, I.E. Wachs, Journal of Catalysis 129 (1991) 307–312.
[30] D.M. Antonelli, A. Nakashira, J.Y. Ying, Inorganic Chemistry 35 (1996) 3126–3136.
[31] Y. Wang, B.M. Smarsly, I. Djerdj, Chemistry of Materials 22 (2010) 6624–6631.
[32] A. Kubacka, G. Colón, M. Fernández-García, Catalysis Today 143 (2009) 286–292.
[33] S.I. Shah, W. Li, C.-P. Huang, O. Jung, C. Ni, Proceedings of the National Academy of Sciences of the United States of America 99 (2002) 6482–6486.
[34] L.R. Sheppard, T. Bak, J. Nowotny, Journal of Physical Chemistry B 110 (2006) 22447–22454.
[35] W. Zeng, T. Liua, Z. Wang, Sensors and Actuators B: Chemical 166–167 (2012) 141–149.
[36] A. Vantomme, B.L. Su, Studies in Surface Science and Catalysis 165 (2007) 235–238.
[37] M.F. Finol, J. Rooke, B.-L. Su, M. Trentesaux, J.-M. Giraudon, J.-F. Lamonier, Catalysis Today 192 (2012) 154–159.
[38] G. Horvath, K. Kawazoe, Journal of Chemical Engineering of Japan 16 (1983) 470–475.
[39] R.D. Shannon, Acta Crystallographica. Section A, Crystal Physics, Diffraction, Theoretical and General Crystallography 32 (1976) 751–767.
[40] I. Djerdj, A.M. Tonejc, Journal of Alloys and Compounds 413 (2006) 159–174.
[41] M.C. Carotta, M. Ferroni, D. Gnani, V. Guidi, M. Merli, G. Martinelli, M.C. Casale, M. Notaro, Sensors and Actuators B: Chemical 58 (1999) 310–317.
[42] M.Z. Atashbar, H.T. Sun, B. Gong, W. Wlodarski, R. Lamb, Thin Solid Films 326 (1998) 238–244.
[43] D. Morris, Y. Dou, J. Rebane, C.E.J. Mitchell, R.G. Egdell, D.S.L. Law, A. Vitadini, M. Casarin, Physical Review B 61 (2000) 13445–13457.
[44] L. Sheppard, T. Bak, J. Nowotny, C.C. Sorrell, S. Kumar, A.R. Gerson, M.C. Barnes, C. Ball, Thin Solid Films 510 (2006) 119–124.
[45] P. Stefanov, M. Shipochka, P. Stefchev, Z. Raicheva, V. Lazarova, L. Spassov, Journal of Physics: Conference Series 100 (2008) 012039.
[46] J.C. Conesa, J. Sorla, Journal of Physical Chemistry 86 (1982) 1392–1395.
[47] S.J. Tauster, S.C. Fung, R.T.K. Baker, J.A. Horsley, Science 211 (1981) 1121–1125.
[48] T. Barakat, J.C. Rooke, M.F. Finol, R. Cousin, J.-F. Lamonier, J.-M. Giraudon, B.-L. Su, S. Siffert, European Journal of Inorganic Chemistry 2012 (2012) 2812–2818.
[49] M. Hosseini, L.H. Tidahy, S. Siffert, R. Cousin, A. Aboukaïs, B.L. Su, Studies in Surface Science and Catalysis 174 (2008) 1323–1326.
[50] M.P. Kapoor, Y. Ichihashi, W.J. Shen, Y. Matsumura, Catalysis Letters 76 (2001) 139–142.
[51] W. Lin, L. Lin, Y.X. Zhu, Y.C. Xie, K. Scheurell, E. Kemnitz, Journal of Molecular Catalysis A 226 (2005) 263–268.
[52] J. Arbiol, J. Cerdà, G. Dezanneau, A. Cirera, F. Peiró, A. Cornet, J.R. Morante, Journal of Applied Physics 92 (2002) 853–861.
[53] F.B. Noronha, D.A.G. Aranda, A.P. Ordine, M. Schmal, Catalysis Today 57 (2000) 275–282.